https://doi.org/10.5194/bg-2023-26
Preprint. Discussion started: 9 February 2023

Biogeosciences
Discussions
Open Access

Alkalinity biases in CMIP6 Earth System Models and implications for simulated CO2 drawdown via artificial alkalinity enhancement

Claudia Hinrichs[1,2], Peter Köhler[1], Christoph Völker1, Judith Hauck[1]

[1] Alfred Wegener Institute, Helmholtz Centre for Polar and Marine Research, 27570 Bremerhaven, Germany
[2] now at: Federal Maritime and Hydrographic Agency (BSH), 20359 Hamburg, Germany

Correspondence to: Claudia Hinrichs (Claudia.Hinrichs@bsh.de)

Abstract. The partitioning of CO_2 between atmosphere and ocean depends to a large degree not only on the amount of dissolved inorganic carbon (DIC) but also of alkalinity in the surface ocean. That is also why, in the context of negative emission approaches ocean alkalinity enhancement is discussed as one potential approach. Although alkalinity is thus an important variable of the marine carbonate system little knowledge exists how its representation in models compares with measurements. We evaluated the large-scale alkalinity distribution in 14 CMIP6 models against the observational data set GLODAPv2 and showed that most models as well as the multi-model-mean underestimate alkalinity at the surface and in the upper ocean, while overestimating alkalinity in the deeper ocean. The decomposition of the global mean alkalinity biases into contributions from physical processes (preformed alkalinity), remineralization, and carbonate formation and dissolution showed that the bias stemming from the physical redistribution of alkalinity is dominant. However, below the upper few hundred meters the bias from carbonate dissolution can become similarly important as physical biases, while the contribution from remineralization processes is negligible. This highlights the critical need for better understanding and quantification of processes driving calcium carbonate dissolution in microenvironments above the saturation horizons, and implementation of these processes into biogeochemical models.

For the application of the models to assess the potential of ocean alkalinity enhancement to increase ocean carbon uptake and counteract ocean acidification, a back-of-the-envelope calculation was conducted with each model's global mean surface alkalinity and DIC as input parameters. We find that the degree of compensation of DIC and alkalinity biases at the surface is more important for the marine CO_2 uptake capacity than the alkalinity biases themselves. The global mean surface alkalinity bias relative to GLODAPv2 in the different models ranges from -85 mmol kg^{-1} (-3.6%) to +50 mmol kg^{-1} (+2.1%) (mean: -25 mmol kg^{-1} or -1.1%), while for DIC the relative bias ranges from -55 mmol kg^{-1} (-2.6%) to 53 mmol kg^{-1} (+2.5%) (mean: -13 mmol kg^{-1} or -0.6%). Because of this partial compensation, all but two of the CMIP6 models evaluated here overestimate the Revelle factor at the surface and thus overestimate the CO_2-draw-down after alkalinity addition by up to 13% and pH increase by up to 7.2%. This overestimate has to be taken into account when reporting on efficiencies of ocean alkalinity enhancement experiments using CMIP6 models.

Plain text summary

https://doi.org/10.5194/bg-2023-26
Preprint. Discussion started: 9 February 2023

This study evaluated the alkalinity distribution in 14 climate models and found that most models underestimate alkalinity at the surface and overestimate in the deeper ocean. It highlights the need for better understanding and quantification of processes driving alkalinity distribution and calcium carbonate dissolution and the importance of accounting for biases in model results when evaluating potential ocean alkalinity enhancement experiments.

1 Introduction

The carbon dioxide (CO_2) concentration in the atmosphere is largely determined by the marine carbonate system in the surface ocean since the partitioning of CO_2 between atmosphere and ocean depends to a large degree on the amount of DIC and alkalinity in the surface ocean (Zeebe and Wolf-Gladrow, 2001). Since preindustrial times the ocean has taken up about a quarter of the anthropogenic CO_2 emitted into the atmosphere (Friedlingstein et al., 2022). Once in the ocean, most of the aqueous CO_2 is converted into bicarbonate (HCO_3^-) and carbonate (CO_3^{2-}) ions, the two other carbonate species of the so-called dissolved inorganic carbon (DIC). The oceanic uptake of anthropogenic carbon leads to an increase in aqueous CO_2 and total DIC and decreases ocean pH, and thus to a change in the chemical equilibria between the carbonate species. Total Alkalinity (TA), a measure of the excess of bases (proton acceptors) over acids, plays a central role in determining how much of the DIC pool exists in the form of CO_2, which is the only of the three marine carbonate species which can exchange with the atmosphere. The overall effect of the carbonate chemistry on the marine uptake capacity of anthropogenic CO_2 emissions is called the buffering capacity of seawater - also known as the Revelle factor, where a low Revelle factor indicates a high buffering capacity and vice versa (Revelle and Suess, 1957, Middelburg et al., 2020). This implies that the resulting change in pH and CO_2 from the same process, e.g., carbonate dissolution, differs depending on the background conditions in TA and DIC (Middleburg et al., 2020). Any changes in pH and CO_2 would be smaller in low-sensitivity or well-buffered seawater with a high TA:DIC ratio (low Revelle factor). That is why when Earth System Models (ESMs) are used to quantify the CO_2 uptake potential of the ocean, it is important to know the initial states of TA and DIC in the models.

In 2015, the 'Paris Agreement' was adopted by 196 governments at the Conference-of-Parties 21 (COP21). Its goal is to restrict human-induced global warming to well below 2°C, preferably to 1.5°C, compared to preindustrial levels. To accomplish this goal, the signing countries aim to reach peak emissions as quickly as possible and to achieve carbon neutrality by the mid-21st century. This goal is likely not achievable through carbon emission reductions alone according to socio-economic scenario simulations with Integrated Assessment Models (Rogelj et al., 2018). The IPCC Special Report on Global Warming of 1.5°C states that all (most) projected pathways that limit warming to 1.5°C (2°C) also require use of carbon dioxide removal (CDR) or negative emission technologies (NETs), on the order of 100–1000 Gt CO_2 over the 21st century (Rogelj et al., 2018). Existing and potential CDR measures are afforestation and reforestation, land restoration and soil carbon sequestration, bioenergy with carbon capture and storage (BECCS), direct air carbon capture and storage (DACCS), enhanced weathering and ocean alkalinization (Gattuso et al., 2018; de Coninck et al., 2018; Board and National Academies of Sciences, 2019; National Academies of Sciences, 2021). So far, much research has been focused on land-based CDR measures and it has become clear that it would be extremely difficult to limit global warming to the agreed level with land-based NETs alone (Fuss et al., 2018;

Lawrence et al., 2018; Smith et al., 2016). Less is known about ocean-based NETs, although some of them appear promising, especially with respect to the potential scale of application (Gattuso et al., 2018; Boettcher et al., 2019). One promising pathway could be ocean alkalinity enhancement (OAE) (Köhler et al., 2013, Renforth and Henderson, 2017). This method is an accelerated version of a natural process: silicate weathering, where alkaline minerals can be mined and crushed (e.g., olivine) or created (e.g., lime) and added to the surface ocean. Alternatively, alkaline solutions from electrochemical weathering can be added. In both scenarios, the alkalinity of the upper ocean is increased and with it the carbon storage capacity of seawater, which leads to an increased uptake of CO_2 from the atmosphere. Aside from lab experiments (Hartmann et al., 2022) and first results from microcosm experiments (Ferderer et al., 2022), these OAE applications are untested at larger scales, so that simulations with state-of-the-art Earth System Models (ESMs) are essential for assessing the efficiency and biogeochemical implications of ocean alkalinization. Previous model experiments have provided first estimates of the efficiency for idealized experiment set-ups, e.g., Ilyina et al. (2013), Köhler et al. (2013), Keller et al. (2014), Hauck et al. (2016), González and Ilyina (2016), Lenton et al. (2018), or Burt et al. (2021). Although these modeling studies have suggested that OAE may be a viable method to help reduce atmospheric CO_2, the results are difficult to compare due to different experimental designs. Another caveat is that previous estimates of OAE efficiency and side effects were based on single model experiments and did not include a thorough assessment of simulated alkalinity and model-dependence of the results. Now, more and more projects are underway or in planning that seek to apply more realistic scenarios for OAE e.g., Butenschön et al. (2021), which is why a model evaluation is even more important.

There have been a number of studies that evaluate the simulation of ocean biogeochemical parameters in state-of-the-art Earth System Models (ESMs) that contributed to CMIP6, the 6th phase of the Coupled Model Intercomparison Project (Eyring et al., 2016), but did not include the evaluation of alkalinity (Séférian et al. (2020), Tagliabue et al. (2021), Kwiatkowski et al. (2020)) or if so then only with one global score number (Fu et al., 2022). The recent study by Planchat et al. (2022) assessed simulated alkalinity and parameters related to the carbonate pump in CMIP6 models and their predecessor CMIP5 versions. They report a significant improvement in the representation of alkalinity and the carbonate pump in CMIP6 versus CMIP5. While some models did increase in complexity, they find that potential effects of future ocean changes (e.g., ocean acidification) are not well constrained in many models.

Here we present further analyses of biases in alkalinity and DIC in CMIP6 models. We show how those biases can be attributed to the ocean's physical, soft-tissue, or carbonate counter pump following Koeve et al. (2014). Furthermore, we provide an estimate of each model's carbonate system sensitivity to OAE depending on their alkalinity and DIC bias in historical simulations.

2. Methods

2.1. CMIP6 models and observational data products

Our evaluation includes 14 ESMs with ocean biogeochemistry modules from ten modelling centers that contributed to CMIP6 and that provided the variables *dissic* (DIC [mol m^{-3}]), *no3* (nitrate concentration [mol m^{-3}]), *o2* (dissolved

https://doi.org/10.5194/bg-2023-26
Preprint. Discussion started: 9 February 2023

oxygen concentration [mol m^{-3}]), *ph* (seawater pH on total scale), *po4* (phosphate concentration [mol m^{-3}]), *so* (salinity (S) [g kg^{-1}]), *talk* (TA [mol m^{-3}]), and *thetao* (potential temperature [°C]), Table 1).

Table 1: Overview of CMIP6 models considered in this study showing the climate model name and description paper, the model ocean component, the model biogeochemistry component, horizontal grid resolution, number of vertical levels, and data reference

CMIP6 ESM	**Ocean Model**	**Ocean Biochem. Model**	**Ocean Horizontal Resolution (lon x lat)**	**Ocean vertical levels**	**Dataset Reference**
ACCESS-ESM-1.5 (Ziehn et al., 2020)	MOM5	WOMBAT	360 x 300 (~1°)	50	(Ziehn et al., 2019)
CanESM5 (Swart et al., 2019b)	NEMO3.4.1 (ORCA1)	CMOC	361 x 290 (~1°)	45	(Swart et al., 2019a)
CESM2 (Danabasoglu et al., 2020)	POP2	MARBL	320 x 384 (~1°)	60	(Danabasoglu, 2019a)
CESM2-WACCM (Danabasoglu et al., 2020)	POP2	MARBL	320 x 384 (~1°)	60	(Danabasoglu, 2019b)
CNRM-ESM-2-1 (Séférian et al., 2019)	NEMO 3.6 (eORCA1)	PISCES 2.s	362 x 294 (~1°)	75	(Seferian, 2018)
GFDL-CM4 (Held et al., 2019; Dunne et al., 2020a)	MOM6	GFDL-BLINGv2	1440 x 1080 (~ 0.25°)	75	(Guo et al., 2018)
GFDL-ESM4 (Dunne et al., 2020b)	MOM6	GFDL-COBALTv2	720 x 576 (~0.5°)	75	(Krasting et al., 2018)
IPSL-CM6A-LR (Boucher et al., 2020)	NEMO-OPA (eORCA1.3)	NEMO-PISCES	362 x 332 (~1°)	75	(Boucher et al., 2018)
MPI-ESM1-2-HR (Müller et al., 2018; Mauritsen et al., 2019)	MPIOM1.63	HAMOCC6	802 x 404 (~0.4°)	40	(Jungclaus et al., 2019)
MPI-ESM1-2-LR (Mauritsen et al., 2019)	MPIOM1.63	HAMOCC6	256 x 220 (~1.5°)	40	(Wieners et al., 2019)
MRI-ESM2-0 (Yukimoto et al., 2019a)	MRI.COM4.4	MRI.COM4.4	360 x 364 (~1°)	61	(Yukimoto et al., 2019b)
NorESM2-LM (Tjiputra et al., 2020)	MICOM	HAMOCC	360 x 384 (~1°)	70	(Seland et al., 2019)
NorESM2-MM (Tjiputra et al., 2020)	MICOM	HAMOCC	360 x 384 (~1°)	70	(Bentsen et al., 2019)
UKESM1-0-LL (Sellar et al., 2019)	NEMO-HadGEM3-GO6.0 (eORCA1)	MEDUSA2	360 x 330 (~1°)	75	(Tang et al., 2019)

For the 14 CMIP6 models, monthly data from the first available ensemble member of the historical simulation was downloaded from the CMIP6 archive (https://esgf-data.dkrz.de), post-processed and regridded with bilinear remapping onto a common 1°x1° grid using Climate Data Operators (cdo, Schulzweida (2022)). Salinity normalization of alkalinity was achieved by using a reference salinity of 35 g kg^{-1}:

$$TA_n = \frac{TA}{S} \times 35 \qquad (1)$$

The present-day (1995-2014) model climatologies from the historical simulations are evaluated against gridded observational products, e.g., TA, DIC and pH from the GLODAPv2.2016b Mapped Climatology (in the following GLODAP, Lauvset et al. (2016)), oxygen and nutrients from the World Ocean Atlas 2018 dataset (WOA, Garcia H.E.

https://doi.org/10.5194/bg-2023-26
Preprint. Discussion started: 9 February 2023

(2019)) and GLODAP, and salinity and temperature from the Polar science center Hydrographic Climatology (PHC3.0, Steele et al. (2001)) and WOA. For the evaluation of global mean vertical profiles, the model data is interpolated onto the same 33 vertical levels used in the GLODAP climatology.

2.2. Analysis of the vertical distribution of total alkalinity - the TA* Method

In order to better understand the vertical distribution of modeled alkalinity compared to the observed one, we follow the 'TA* Method' as described by Koeve et al. (2014). This method aims to separate the effects of biogeochemical processes and ocean circulation on the distribution of TA. To achieve this, TA is separated into three components: preformed TA (TA^0), TA decrease from remineralization of organic matter (TA^r), and TA increase due to calcium carbonate ($CaCO_3$) formation and dissolution (TA*):

$$TA = TA^0 + TA^* - TA^r \ [\mathrm{mmol\ m^{-3}}] \quad (2)$$

Preformed TA represents the TA a water parcel had when it was last in contact with the atmosphere. This preformed TA is derived by applying multi-linear regression of upper ocean (here top 100 m) salinity, temperature, and PO (a conservative water-mass tracer analog to NO in Broecker (1974)) for each model, where

$$PO = O_2 + r_{-O2:PO4} \cdot PO_4, \quad (3)$$

with $r_{-O2:PO4} = 170$, onto upper ocean TA values. The obtained regression coefficients are then applied to salinity, potential temperature, and PO everywhere in the interior ocean to compute the model's TA^0 at any location.

The TA^r term describes the reduction of TA stemming from the remineralization of organic matter. This term can be described as a function of the simulated Apparent Oxygen Utilization (AOU, Garcia and Levitus, 2006):

$$TA^r = r_{Alk:NO3} \cdot r_{NO3:-O2} \cdot AOU, \quad (4)$$

with $r_{Alk:NO3} = 1.26$, $r_{NO3:-O2} = 1/10.625$, and AOU as difference between oxygen saturation computed following Weiss (1970) and oxygen concentration O_2.

Lastly, the contribution from carbonate formation and dissolution, TA*, is computed as residual after rearranging Eq. (2).

We applied the TA* Method to 10 of 14 CMIP6 models (CNRM-ESM2-1, GFDL-CM4, GFDL-ESM4, IPSL-CM6A-LR, MPI-ESM1-2-HR, MPI-ESM1-2-LR, MRI-ESM2-0, NorESM2-LM, NorESM2-MM, UKESM1-0-LL), which had the necessary output fields (*talk*, *so*, *thetao*, *o2*, and *po4*).

2.3. Theoretical Model Sensitivity to Alkalinity Enhancement

Systematic biases in TA and DIC have implications for a model's carbonate system sensitivity to added alkalinity during OAE and thus differences in ocean carbon uptake and pH increase may result. In order to evaluate the range of this carbonate system sensitivity we conducted back-of-the-envelope-calculations for all ESMs and the GLODAP dataset using the Matlab toolbox CO2SYS (Lewis et al., 1998; Van Heuven et al., 2011). This toolbox computes the remaining parameters of the carbonate system in seawater based on two input parameters. Here, we use the time and area-weighted mean surface TA and DIC converted from mmol m^{-3} to µmol kg^{-1} with a density of 1026 kg m^{-3}, see Figure 1 for individual values. We evaluate the CO2SYS output fields Revelle Factor, pH, and pCO_2 (partial pressure of CO_2 in seawater) based on the CMIP6 output and additionally the changes in pCO_2 after an addition of 100 µmol kg^{-1} TA against GLODAP observations.

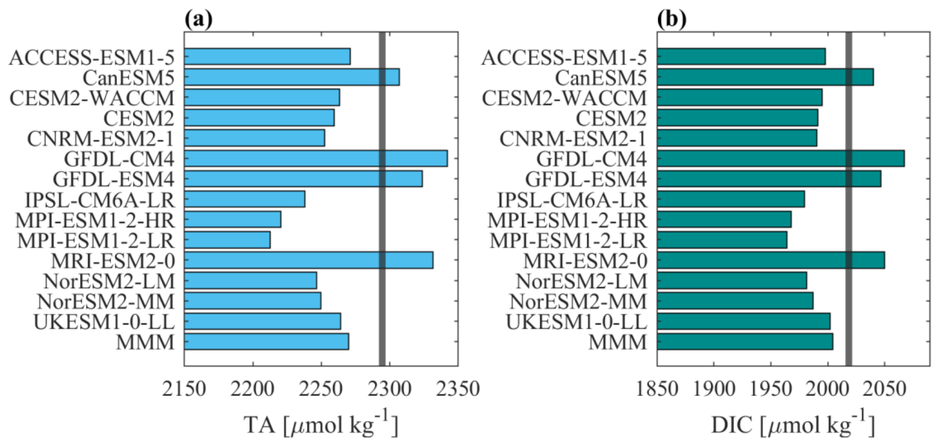

Figure 1: (a) Global mean surface total alkalinity (TA) of the 14 CMIP6 models and the multi-model-mean (MMM), black vertical line indicates GLODAP value, (b) same for dissolved inorganic carbon (DIC).

Additionally, we use the following values for the computation of the carbonate systems: salinity = 34.0, temperature = 15 °C, silicic acid = 2 µmol kg^{-1}, and phosphate = 1 µmol kg^{-1}. Gas exchange with the atmosphere is not considered in this exercise.

3. Results

3.1. Analysis of CMIP6 alkalinity and DIC

The comparison of the models' simulated TA at the ocean surface to the GLODAP climatology shows that – on a global scale - most models underestimate surface TA, except for four models, CanESM5, GFDL-CM4, GFDL-ESM4 and MRI-ESM2-0, which simulate too much TA at the surface. The multi-model-mean (MMM) is slightly negatively biased (Figure 2). Near-surface TA is strongly correlated to salinity, and upper ocean salinity is governed by freshwater fluxes, e.g., precipitation and evaporation (Millero et al., 1998), and river flows (Cai et al., 2010). Thus, TA is often normalized with salinity to exclude the freshwater effect in the alkalinity assessment (Millero et al., 1998; Fry et al., 2015). Overall, the comparison of salinity-normalized TA to GLODAP data shows bias patterns very similar to those of TA for all models. Most notably, some regional peculiarities that stem from salinity biases rather than biogeochemical processes are smoothed out (e.g., North Atlantic bias in NorESM) (Figure S1).

https://doi.org/10.5194/bg-2023-26
Preprint. Discussion started: 9 February 2023

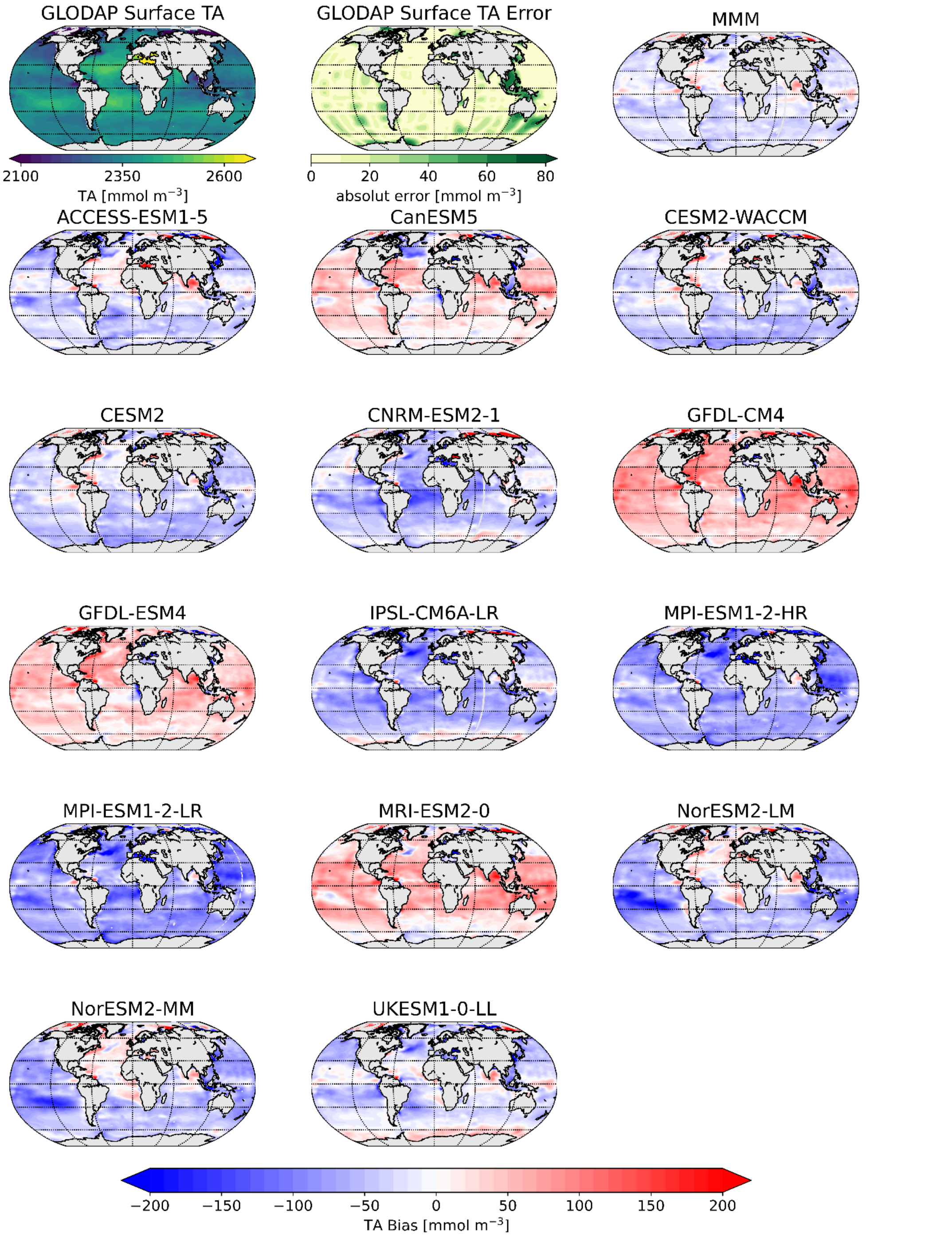

Figure 2: Surface distribution of total alkalinity [TA, mmol m^{-3}] in GLODAP (top left) as well as its error estimate (top center), and the CMIP6 multi-model-mean (MMM) bias (top right) as well as the individual model's biases.

https://doi.org/10.5194/bg-2023-26
Preprint. Discussion started: 9 February 2023

Biogeosciences
Discussions

The vertical profiles of globally averaged TA and normalized TA (Figure 3) show the aforementioned distribution of the CMIP6 models' surface bias as well, with most of the models showing less surface TA than GLODAP. The models mostly reproduce the features of the observed TA depth profile: the surface minimum, the subsurface maximum of TA, another minimum at around 500 m depth and the increase of TA with depth below that (Figure 3a). Two models of the same family (MPI-ESM1-2-LR and MPI-ESM1-2-HR) have less TA than the GLODAP product over the whole water column and two models (GFDL-CM4 and GFDL-ESM4) have higher TA overall indicating that their global inventory of TA is too low (too high) compared to GLODAP. The explanation for the systematic low bias in the MPI model seems to be that too much TA was lost to the sediments during the model spin up (Koeve et al., 2014; Planchat et al., 2022). The high TA bias in the GFDL model was apparently introduced in the post-processing step during the unit conversion from gravimetric (μmol kg^{-1}) to volumetric (mmol m^{-3}, common SI unit). The unit conversion is usually based on a chosen density value which is not prescribed in modeling protocols. While most models chose a value between 1024 kg m^{-3} and 1028 kg m^{-3}, the modeling group at GFDL apparently converted the units using a value of 1035 kg m^{-3} (Planchat et al., 2022). The profiles of the other models show either too little TA at the surface and too much at depth or vice versa, indicating that their TA inventory is closer to the observed one but that the TA distribution in the water column differs from the observations. Salinity-normalization generally does not change the bias patterns (Figure 3b). The salinity-normalization does affect the shape of the profiles in the upper ocean, where the surface minima and the subsurface maxima seen in TA disappear. Those features are essentially related to the upper ocean salinity distribution.

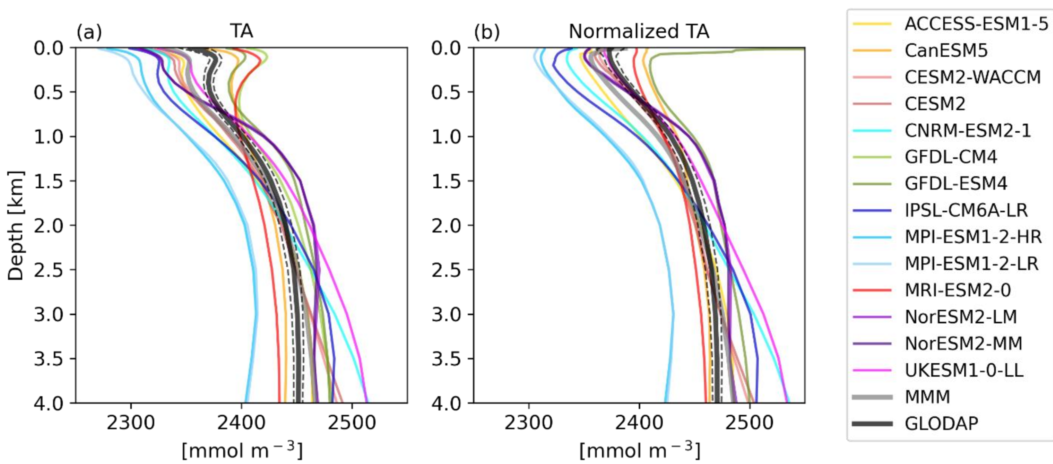

Figure 3: Vertical profiles of global mean TA (a) and salinity-normalized TA (b) of the CMIP6 models, the multi-model-mean (MMM in grey) and GLODAP (black) with error estimate (black dashed lines)

The near-surface TA maximum seen in the global profile is also evident in the Atlantic, Pacific and Indian Oceans (Figure 4). The high TA is related to the salinity maxima of subtropical underwater in the respective basins (Talley, 2002) and all models replicate this pattern. In the Atlantic Ocean, a TA minimum can be observed in the GLODAP data at around 800 m depth which represents Antarctic Intermediate Water in the South Atlantic (low salinity)

https://doi.org/10.5194/bg-2023-26
Preprint. Discussion started: 9 February 2023

Biogeosciences
Discussions
Open Access

(Takahashi et al., 1981). This minimum is not well reproduced by the ESMs. The relatively low TA in the deep Atlantic Ocean (compared to the Pacific and Indian Ocean) between 1,500 m and 3,500 m depth and the small gradient with depth is linked to North Atlantic Deep Water. Most models reproduce this pattern, while the CNRM, IPSL and UK ESMs simulate a strong increase of TA below about 2,000 m depth (Figure 4b). The profile shapes in the Southern Ocean and Arctic Ocean are generally reproduced in terms of the TA gradients with depths, albeit the biases in absolute amount of TA present are visible here as well.

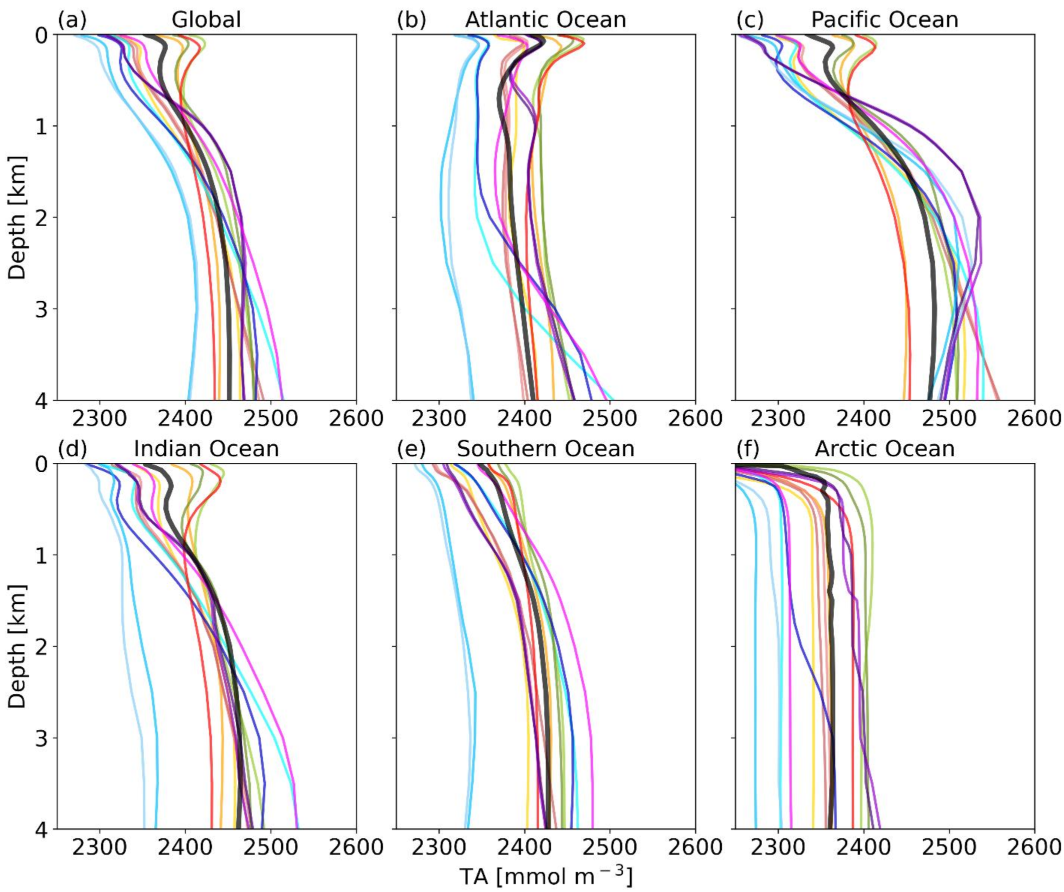

Figure 4: Global mean TA profiles for the major ocean basins. Color assignment is the same as in Figure 3.

The surface DIC patterns compared to GLODAP show very similar patterns to those for TA, both in general direction und local distribution (Figure 5). The global mean surface biases in TA compared to GLODAP range from -85 mmol m^{-3} (-3.6 %) to +50 mmol m^{-3} (+2.1 %), where the MMM bias is -25 mmol m^{-3} (-1.1 %) and for the global mean surface DIC the biases range from -55 mmol m^{-3} (-2.6 %) to 53 mmol m^{-3} (+2.5 %), with the MMM bias being -13 mmol m^{-3} (-0.6 %). TA biases likely lead DIC biases, as DIC can adjust through gas-exchange of CO_2. Models with higher TA have higher DIC values and vice versa. We next investigate the origin of the models' alkalinity biases.

https://doi.org/10.5194/bg-2023-26
Preprint. Discussion started: 9 February 2023

Biogeosciences
Discussions

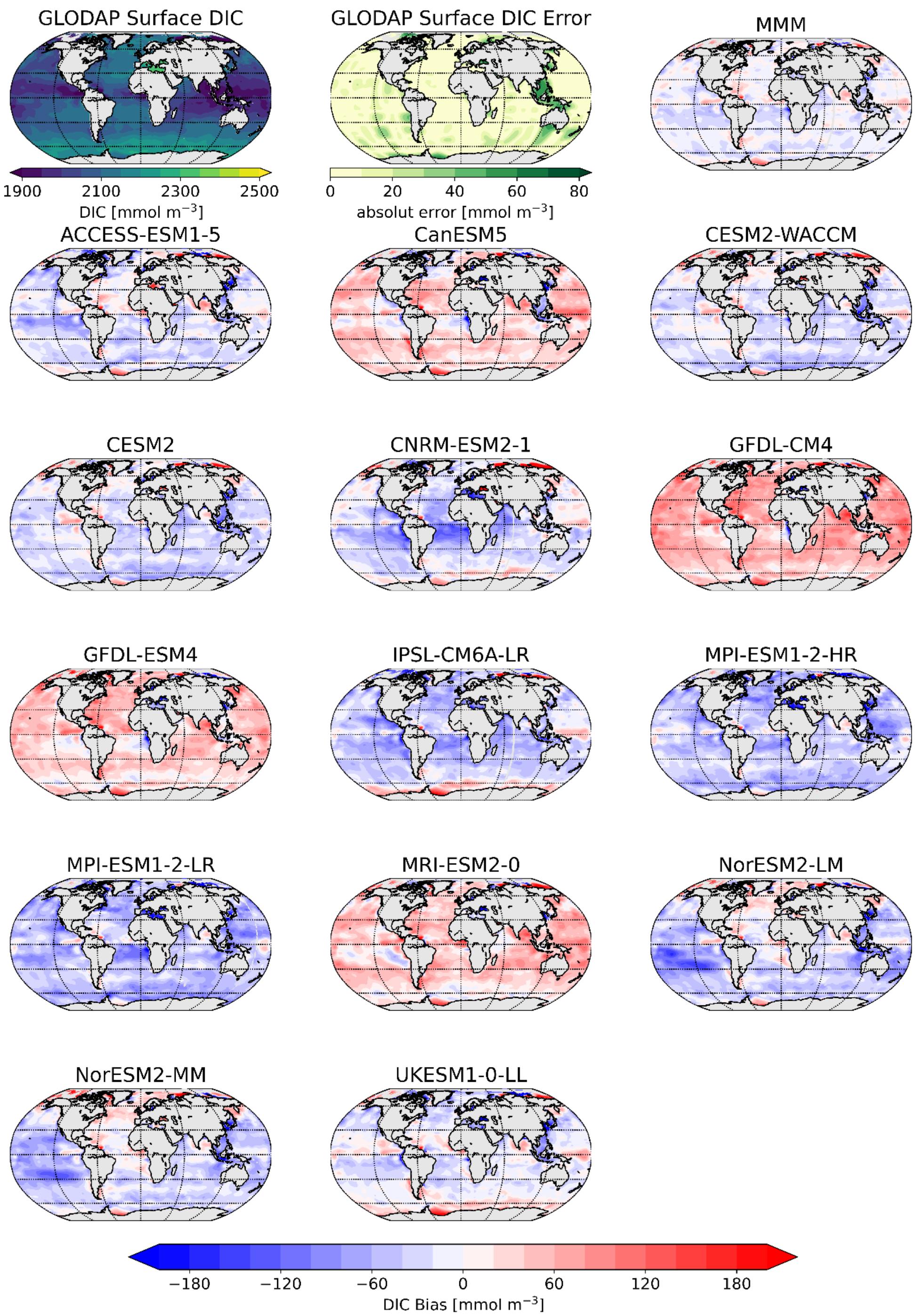

215 *Figure 5: Surface distribution of DIC in GLODAP as well as its error estimate, and the CMIP6 multi-model-mean (MMM, top right) bias as well as the individual models' biases.*

https://doi.org/10.5194/bg-2023-26
Preprint. Discussion started: 9 February 2023

3.2. Analysis of the vertical alkalinity distribution

The goal of the 'TA* Method' (Koeve et al., 2014) is to separate the TA bias into contributions from 1) an inadequate representation of ocean physics or forcings (e.g., circulation, freshwater flow, evaporation, and precipitation), 2) the parametrization of calcium carbonate ($CaCO_3$) formation and dissolution and 3) the parametrization of organic matter remineralization processes.

The vertical distribution of the TA bias with respect to GLODAP and its components according to the TA* method are shown in Figure 6. The MPI models have too little TA at all water depths. The IPSL-CM6A-LR, CNRM-ESM2-1, the NorESM2 models and the UKESM1 model underestimate upper ocean TA and overestimate TA at depth. The MRI-ESM2-0 overestimates TA in the upper ocean and underestimates it at depths below ~ 1,000 m. Both GFDL models contain too much TA at all depths for the above explained reason of a too high seawater density during units conversion. In the upper 1 km most of the models' alkalinity biases are due to their preformed TA (Figure 6b). This also implies that the subsurface maxima and minima in the observed TA profile are due to preformed TA and not related to biogeochemical modifications of TA. Biases in the representation of organic matter remineralization processes play a negligible role (Figure 6c), while for some models the bias in TA from calcium carbonate dissolution in the interior ocean (Figure 6d) is in absolute terms comparable to or even larger than the bias in preformed TA.

https://doi.org/10.5194/bg-2023-26
Preprint. Discussion started: 9 February 2023

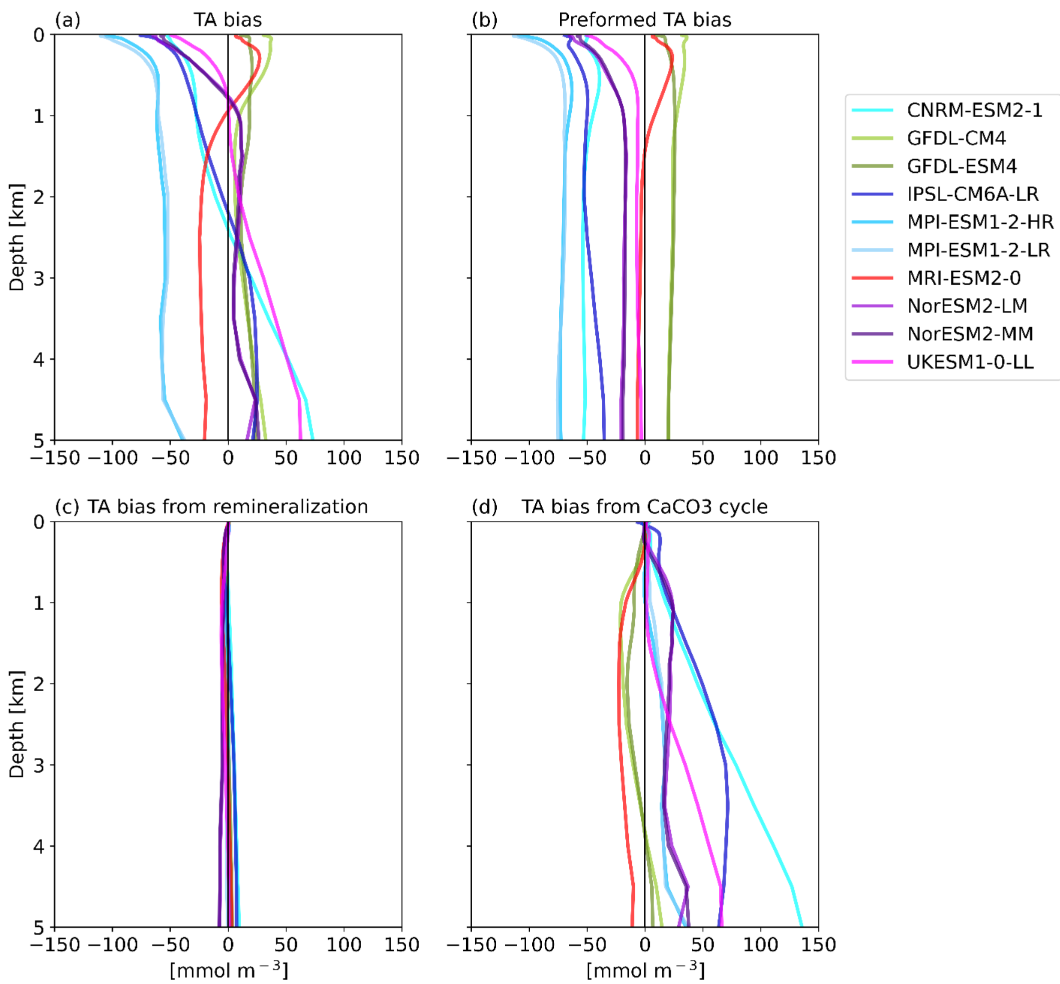

Figure 6: Globally averaged depth profiles of biases in TA, preformed TA (TA^0), TA from remineralization (TA^r) and from calcium carbonate formation and dissolution (TA) in 10 CMIP6 models compared to the GLODAP climatology.*

3.3. Impact of biases on efficiency of ocean alkalinity enhancement

Biases in simulated surface TA and surface DIC have implications for the individual models' efficiency of OAE in terms of change in pCO_2 and pH and thus in the marine CO_2 uptake capacity. In order to evaluate the range of this sensitivity, a back-of-the-envelope-calculation was conducted to calculate the full carbonate system from two input parameters (global mean surface TA and DIC in µmol kg^{-1}) (see Methods, see Figure 1 for input values). Results from this calculation together with the models' TA-to-DIC-ratio are shown in Figure 7. All panels are sorted by Revelle Factor in ascending order. The Revelle factor or buffer factor describes the ocean's capability to take up atmospheric CO_2. It is the ratio of instantaneous change in pCO_2 to the change in DIC at the ocean surface. Depending on the state

https://doi.org/10.5194/bg-2023-26
Preprint. Discussion started: 9 February 2023

Biogeosciences
Discussions

of the carbonate system, which is fully described by DIC and TA, the speciation of DIC into the three carbonate species CO_3^{2-}, HCO_3^-, and CO_2 is determined. The lower the Revelle factor, the greater is the buffering capacity and the more DIC occurs as CO_3^{2-} or HCO_3^-, effectively lowering the pCO_2 levels in the ocean. This allows the ocean to take up more CO_2 which in turn also lowers atmospheric pCO_2 (Egleston et al., 2010).

The global mean Revelle Factor from the CO2SYS computation for the GLODAP dataset is the third lowest in our compilation, 10.19, and thus almost all models have a higher Revelle Factor than GLODAP data suggest ranging from 10.18 to 10.54 (Figure 7a). The Revelle factor is anti-correlated to the average TA-to-DIC-ratio (Figure 7b). Also, the order of relative surface pH (Figure 7c) and pCO_2 (Figure 7d) values corresponds largely to each model's rank in Revelle Factor and TA-DIC-ratio. Models with a higher Revelle factor than GLODAP have a lower buffer capacity which leads to already higher pCO_2 values (290 to 314 µatm) and lower pH (8.12 to 8.17) than observed in GLODAP (pCO_2: 292 µatm, pH: 8.16). Those models also show a greater decrease in pCO_2 for the hypothetical addition of 100 µmol kg^{-1} of TA (Figure 7e) than GLODAP (-92 µatm), ranging from a 91 µatm to a 104 µatm decrease in pCO2 .

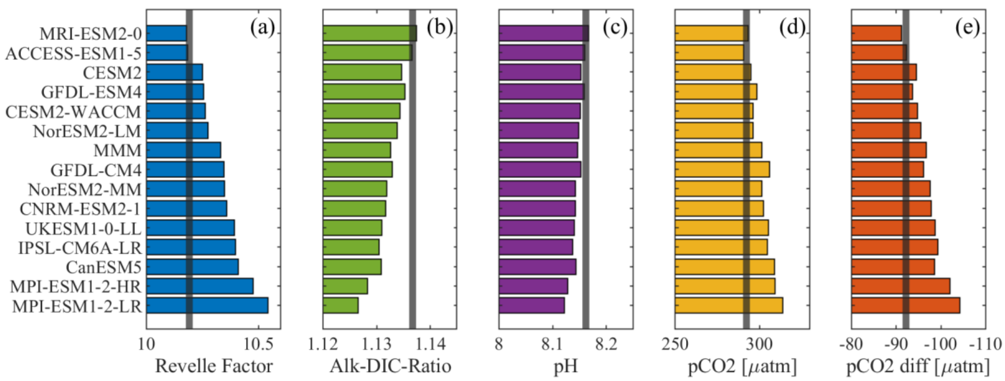

Figure 7: Carbonate system parameters were computed for all models, the multi-model-mean (MMM) and the GLODAP data (grey line) with the CO2SYS toolbox, based on the two input parameters global mean alkalinity and DIC. The results are sorted by Revelle Factor in ascending order for all panels. Shown are the Revelle factor (a), the TA-DIC ratio (b) pH (c), pCO_2 (d) and difference in pCO_2 after a 100 µmol kg^{-1} addition of TA.

In relative terms, we find that the ESMs' TA biases range from -3.6% to +2.1% with a mean of -1.1% and their DIC biases ranges from -2.6% to +2.5% with a mean value of -0.6% (Figure 1). Furthermore, the ESMs estimates of the pCO_2 decrease after a hypothetical TA enhancement by 100 µmol kg^{-1} t ranges from -1.0% up to 13.0% (mean 5.1%) (Figure 8). The controlling factor for this pCO_2 bias is in most cases the Revelle factor rather than the TA bias alone, because the TA bias is always accompanied by a compensating DIC bias.

https://doi.org/10.5194/bg-2023-26
Preprint. Discussion started: 9 February 2023

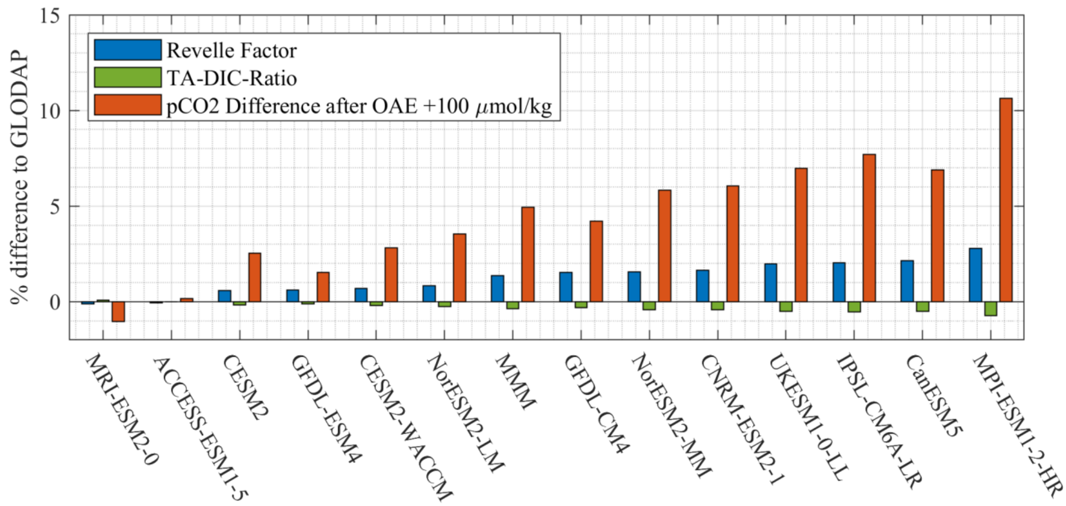

Figure 8: Relative difference of the Revelle factor (blue) and TA-DIC-Ratio (green) to GLODAP, as well as pCO_2 difference after a 100 µmol kg^{-1}-increase in TA (orange) in CMIP6 models and the MMM. The models are sorted by Revelle Factor difference to GLODAP.

This simplified OAE example shows that in 12 out 14 ESMs an increase of 100 µmol kg^{-1} in TA would lead to a higher decrease in pCO_2 than observational data from GLODAP suggest. A higher sensitivity to TA changes due to a higher Revelle factor has also been shown in Hauck et al. (2016) during a decadal scale OAE simulation. We additionally calculated the effect of the additions of 200, 500 and 1,000 µmol kg^{-1} of TA. The degree of CO_2 uptake overestimation decreases with the amount of TA added, but for a theoretical addition of 1,000 µmol kg^{-1} of TA the maximum CO_2 uptake overestimate with respect to GLODAP is still 8% (Table S2). We conclude that almost all ESMs might overestimate the additional CO_2 uptake in simulated OAE experiments.

4. Discussion and conclusions

We evaluated CMIP6 models regarding their large-scale biases in TA and DIC compared to the gridded data set GLODAP. Ten out of 14 ESMs underestimate surface TA (MMM: -25 mmol m^{-3} or -1.1%) and DIC (MMM: -13 mmol m^{-3} or -0.6%) with respect to observations. The range of the bias in TA is -85 mmol m^{-3} (-3.6 %) to 50 mmol m^{-3} (+2.1 %) and in DIC is -55 mmol m^{-3} (-2.6 %) to 53 mmol m^{-3} (+2.5 %). This is a reversal from the TA and DIC representation in CMIP5, where most models and the MMM overestimated these variables, and the absolute and relative errors were at least twice as large as in CMIP6 (Planchat et al., 2022). The direction of the bias and the relative biases of TA and DIC have a direct impact on the buffer capacity of the surface ocean and should be known when assessing model experiments simulating OAE or other NETs that directly affect the ocean's carbonate chemistry. Terhaar et al. (2022) also found that CMIP6 models overestimate the Revelle factor and propose that CMIP6 models underestimate the anthropogenic ocean carbon sink 1994-2007 by 9%, of which around 3% can be explained by the overestimation of the Revelle factor and the remaining 6% are related to the models' underestimation of the Atlantic Meridional overturning circulation.

It is helpful to understand the contributions of the physical and biological - the soft tissue and calcium carbonate - pumps to these TA biases in ESMs. We separated the global mean vertical TA bias into contributions from preformed alkalinity (physical pump), remineralization (soft tissue pump) and alkalinity from calcification and carbonate dissolution ($CaCO_3$ pump) following Koeve et al. (2014). The conclusion from this analysis is that especially in the upper ocean the global distribution of TA in ESMs is largely determined by preformed TA which is set by ocean model physics (advection, overturning, mixing, etc.). Below the upper ocean, biases in TA are also driven by the $CaCO_3$ cycle, while contributions from remineralization are negligible. Although Planchat et al. (2022) do not assess alkalinity biases due to the physical carbon pump, they also point to a larger contribution of the carbonate pump relative to the soft tissue pump (remineralization) to the (normalized) TA biases. The model processes involving the physical distribution of TA are tuned to achieve the best overall model performance and it could be tested whether a tuning to improve TA would support this goal. The findings regarding the contribution to the TA biases from the $CaCO_3$ cycle simulation suggest that improving the parametrizations of biogeochemical processes that are sources and sinks of TA, e.g., calcification, remineralization of sinking detritus, chemical dissolution of calcium carbonate, biological $CaCO_3$ formation and dissolution, etc. would be beneficial. Since the bias in TA from remineralization is small in all models, parametrizations that affect the carbonate chemistry are the most practical lever to improve the TA distribution for most models. This, in turn, needs a much-improved process understanding of $CaCO_3$ dissolution in microenvironments such as aggregates, zooplankton and fish guts above the $CaCO_3$ saturation horizons (Sulpis et al., 2021; Jansen and Wolf-Gladrow, 2001; Salter et al., 2017) from field and laboratory studies in order to mechanistically represent these processes and how they might be altered in a high-CO_2 ocean. In the absence of this mechanistic understanding, some suggestions to reduce TA biases are:

- If TA is low at the surface, decreasing the calcification (rate) within realistic limits or increasing near-surface dissolution could be beneficial (Gangstø et al., 2008; Gehlen et al., 2007).
- If calcite dissolution is formulated as (mostly) saturation-dependent and is therefore (close to) zero above the calcite saturation horizon, a term can be implemented that encompasses dissolution processes that have been observed to occur above said horizon, e.g., calcite dissolution in microenvironments like marine snow and zooplankton guts (Sulpis et al., 2021). It was shown that the acidic environment in guts of starving copepods can dissolve up to 38% of the calcite taken up by grazing (White et al., 2018). For non-starving copepods this value was somewhat lower (Pond et al., 1995; Jansen and Wolf-Gladrow, 2001).
- In addition to those processes, it is known that aragonite and high-magnesium calcite have a shallower saturation horizon than calcite and contribute to upper-ocean calcium carbonate dissolution (Sabine et al., 2002; Gangstø et al., 2008; Barrett et al., 2014; Battaglia et al., 2016), while almost all models only simulate calcite explicitly (Planchat et al. 2022). The carbon cycle formulation could be expanded to also simulate aragonite or more dissolution can be let to occur above the saturation horizon.
- If the calcite dissolution is prescribed to increase with depth (Yamanaka and Tajika, 1996) this process could be tuned with a better match to the observed vertical distributions of calcite or TA.

https://doi.org/10.5194/bg-2023-26
Preprint. Discussion started: 9 February 2023

The back-of-the-envelope calculation of the ESMs' carbonate system states revealed that all but two of models have a higher global mean Revelle Factor than calculated from GLODAP (see also Terhaar et al., 2022), correlated with a higher TA-DIC-ratio than suggested by observations. For a hypothetical addition of 100 µmol kg^{-1} TA this bias leads to an overestimate of the proposed additional CO_2 uptake from the atmosphere by up to 13%. The addition of just 100 µmol kg^{-1} TA is actually at the very low end of the spectrum used in past and current OAE experiments in models and in mesocosms (Hartmann et al., 2022; Ferderer et al., 2022). This calculation is a simplified exercise since gas exchange between ocean and atmosphere is not accounted for nor the potential precipitation and sinking of calcium carbonate (Hartmann et al., 2022). In order to fully capture the effect of OAE on atmospheric CO_2 concentration and the model spread related to biases stemming from circulation and biogeochemical assumptions, these OAE experiments need to be performed in a suite of fully coupled emission-driven ESMs with a precise protocol and with realistic representation of the carbonate pump, including $CaCO_3$ dissolution above the carbonate saturation horizon, which is not even sufficiently understood in the real world (Sulpis et al., 2021).

Acknowledgements

This project has received funding from the European Union's Horizon 2020 research and innovation program under grant agreement number 869357 and from the Initiative and Networking Fund of the Helmholtz Association (Helmholtz Young Investigator Group Marine Carbon and Ecosystem Feedbacks in the Earth System [MarESys], grant number VH-NG-1301) . Furthermore, this work used resources of the Deutsches Klimarechenzentrum (DKRZ) granted by its Scientific Steering Committee (WLA) under project ID ba1103.

Code availability:

The CO2SYS matlab toolbox is available at https://cdiac.ess-dive.lbl.gov/ftp/co2sys/CO2SYS_calc_MATLAB_v1.1/ .

Data availability:

All CMIP6 model output has been downloaded from the data sources given in Table 1.

Author contributions:

JH is PI, CV and PK are co-PIs of this sub-project contributing to the EU project OceanNETs (money aquisition). CH performed the data analysis, preparation of the figures and led the writing of the draft. All co-authors contributed to draft writing by editing the initial version.

References

Barrett, P. M., Resing, J. A., Buck, N. J., Feely, R. A., Bullister, J. L., Buck, C. S., and Landing, W. M.: Calcium carbonate dissolution in the upper 1000 m of the eastern North Atlantic, Global biogeochemical cycles, 28, 386-397, 2014.

Battaglia, G., Steinacher, M., and Joos, F.: A probabilistic assessment of calcium carbonate export and dissolution in the modern ocean, Biogeosciences, 13, 2823-2848, 10.5194/bg-13-2823-2016, 2016.

Bentsen, M., Olivié, D. J. L., Seland, Ø., Toniazzo, T., Gjermundsen, A., Graff, L. S., Debernard, J. B., Gupta, A. K., He, Y., Kirkevåg, A., Schwinger, J., Tjiputra, J., Aas, K. S., Bethke, I., Fan, Y., Griesfeller, J., Grini, A., Guo, C., Ilicak, M., Karset, I. H. H., Landgren, O. A., Liakka, J., Moseid, K. O., Nummelin, A., Spensberger, C., Tang, H., Zhang, Z., Heinze, C., Iversen, T., and Schulz, M.: NCC NorESM2-MM model output prepared for CMIP6 CMIP historical, Earth System Grid Federation [dataset], 10.22033/ESGF/CMIP6.8040, 2019.

Board, O. S. and National Academies of Sciences, E., and Medicine: Negative emissions technologies and reliable sequestration: A research agenda, 2019.

Boettcher, M., Chai, F., Cullen, J., Goeschl, T., Lampitt, R., Lenton, A., Oschlies, A., Rau, G., Rickaby, R., and Ricke, K.: High level review of a wide range of proposed marine geoengineering techniques, 2019.

Boucher, O., Servonnat, J., Albright, A. L., Aumont, O., Balkanski, Y., Bastrikov, V., Bekki, S., Bonnet, R., Bony, S., and Bopp, L.: Presentation and evaluation of the IPSL-CM6A-LR climate model, Journal of Advances in Modeling Earth Systems, 12, e2019MS002010, 2020.

Boucher, O., Denvil, S., Levavasseur, G., Cozic, A., Caubel, A., Foujols, M.-A., Meurdesoif, Y., Cadule, P., Devilliers, M., Ghattas, J., Lebas, N., Lurton, T., Mellul, L., Musat, I., Mignot, J., and Cheruy, F.: IPSL IPSL-CM6A-LR model output prepared for CMIP6 CMIP historical, Earth System Grid Federation [dataset], 10.22033/ESGF/CMIP6.5195, 2018.

Broecker, W. S.: "NO", a conservative water-mass tracer, Earth and Planetary Science Letters, 23, 100-107, 1974.

Cai, W. J., Hu, X., Huang, W. J., Jiang, L. Q., Wang, Y., Peng, T. H., and Zhang, X.: Alkalinity distribution in the western North Atlantic Ocean margins, Journal of Geophysical Research: Oceans, 115, 2010.

Butenschön, M., Lovato, T., Masina, S., Caserini, S., and Grosso, M.: Alkalinization scenarios in the Mediterranean Sea for efficient removal of atmospheric CO2 and the mitigation of ocean acidification, Frontiers in Climate, 3, 614537, 2021.

Danabasoglu, G.: NCAR CESM2 model output prepared for CMIP6 CMIP historical, Earth System Grid Federation [dataset], 10.22033/ESGF/CMIP6.7627, 2019a.

Danabasoglu, G.: NCAR CESM2-WACCM model output prepared for CMIP6 CMIP historical, Earth System Grid Federation [dataset], 10.22033/ESGF/CMIP6.10071, 2019b.

Danabasoglu, G., Lamarque, J.-F., Bacmeister, J., Bailey, D. A., DuVivier, A. K., Edwards, J., Emmons, L. K., Fasullo, J., Garcia, R., Gettelman, A., Hannay, C., Holland, M. M., Large, W. G., Lauritzen, P. H., Lawrence, D. M., Lenaerts, J. T. M., Lindsay, K., Lipscomb, W. H., Mills, M. J., Neale, R., Oleson, K. W., Otto-Bliesner, B., Phillips, A. S., Sacks, W., Tilmes, S., van Kampenhout, L., Vertenstein, M., Bertini, A., Dennis, J., Deser, C., Fischer, C., Fox-Kemper, B., Kay, J. E., Kinnison, D., Kushner, P. J., Larson, V. E., Long, M. C., Mickelson, S., Moore, J. K., Nienhouse, E., Polvani, L., Rasch, P. J., and Strand, W. G.: The Community Earth System Model Version 2 (CESM2), Journal of Advances in Modeling Earth Systems, 12, e2019MS001916, https://doi.org/10.1029/2019MS001916, 2020.

de Coninck, H., Revi, A., Babiker, M., Bertoldi, P., Buckeridge, M., Cartwright, A., Dong, W., Ford, J., Fuss, S., and Hourcade, J.-C.: Strengthening and implementing the global response, in: Global warming of 1.5 C: Summary for policy makers, IPCC-The Intergovernmental Panel on Climate Change, 313-443, 2018.

Dunne, J. P., Bociu, I., Bronselaer, B., Guo, H., John, J., Krasting, J., Stock, C., Winton, M., and Zadeh, N.: Simple global ocean Biogeochemistry with Light, Iron, Nutrients and Gas version 2 (BLINGv2): Model description and simulation characteristics in GFDL's CM4. 0, Journal of Advances in Modeling Earth Systems, 12, e2019MS002008, 2020a.

Dunne, J. P., Horowitz, L. W., Adcroft, A. J., Ginoux, P., Held, I. M., John, J. G., Krasting, J. P., Malyshev, S., Naik, V., Paulot, F., Shevliakova, E., Stock, C. A., Zadeh, N., Balaji, V., Blanton, C., Dunne, K. A., Dupuis, C., Durachta, J., Dussin, R., Gauthier, P. P. G., Griffies, S. M., Guo, H., Hallberg, R. W., Harrison, M., He, J., Hurlin, W., McHugh, C., Menzel, R., Milly, P. C. D., Nikonov, S., Paynter, D. J., Ploshay, J., Radhakrishnan, A., Rand, K., Reichl, B. G., Robinson, T., Schwarzkopf, D. M., Sentman, L. T., Underwood, S., Vahlenkamp, H., Winton, M., Wittenberg, A. T., Wyman, B., Zeng, Y., and Zhao, M.: The GFDL Earth System Model Version 4.1 (GFDL-ESM 4.1): Overall Coupled Model Description and Simulation Characteristics, Journal of Advances in Modeling Earth Systems, 12, e2019MS002015, https://doi.org/10.1029/2019MS002015, 2020b.

Egleston, E. S., Sabine, C. L., and Morel, F. M.: Revelle revisited: Buffer factors that quantify the response of ocean chemistry to changes in DIC and alkalinity, Global Biogeochemical Cycles, 24, 2010.
Eyring, V., Bony, S., Meehl, G. A., Senior, C. A., Stevens, B., Stouffer, R. J., and Taylor, K. E.: Overview of the Coupled Model Intercomparison Project Phase 6 (CMIP6) experimental design and organization, Geoscientific Model Development, 9, 1937-1958, 2016.
Ferderer, A., Chase, Z., Kennedy, F., Schulz, K. G., and Bach, L. T.: Assessing the influence of ocean alkalinity enhancement on a coastal phytoplankton community, Biogeosciences, 19, 5375–5399, 2022.
Friedlingstein, P., O'Sullivan, M., Jones, M. W., Andrew, R. M., Gregor, L., Hauck, J., Le Quéré, C., Luijkx, I. T., Olsen, A., and Peters, G. P.: Global carbon budget 2022, Earth System Science Data, 14, 4811–4900, 2022.
Fry, C. H., Tyrrell, T., Hain, M. P., Bates, N. R., and Achterberg, E. P.: Analysis of global surface ocean alkalinity to determine controlling processes, Marine Chemistry, 174, 46-57, https://doi.org/10.1016/j.marchem.2015.05.003, 2015.
Fu, W., Moore, J. K., Primeau, F., Collier, N., Ogunro, O. O., Hoffman, F. M., & Randerson, J. T.: Evaluation of ocean biogeochemistry and carbon cycling in CMIP earth system models with the International Ocean Model Benchmarking (IOMB) software system. Journal of Geophysical Research: Oceans, 127, e2022JC018965. https://doi.org/10.1029/2022JC018965, 2022.
Fuss, S., Lamb, W. F., Callaghan, M. W., Hilaire, J., Creutzig, F., Amann, T., Beringer, T., de Oliveira Garcia, W., Hartmann, J., and Khanna, T.: Negative emissions—Part 2: Costs, potentials and side effects, Environmental Research Letters, 13, 063002, 2018.
Gangstø, R., Gehlen, M., Schneider, B., Bopp, L., Aumont, O., and Joos, F.: Modeling the marine aragonite cycle: changes under rising carbon dioxide and its role in shallow water CaCO 3 dissolution, Biogeosciences, 5, 1057–1072, 2008.
Garcia, H. E. and Levitus, S.: World ocean atlas 2005. Vol. 3, Dissolved oxygen, apparent oxygen utilization, and oxygen saturation, 2006.
Garcia H.E., T. P. B., O.K. Baranova, R.A. Locarnini, A.V. Mishonov, A. Grodsky, C.R. Paver, K.W. Weathers, I.V. Smolyar, J.R. Reagan, D. Seidov, M.M. Zweng: World Ocean Atlas 2018: Product Documentation [dataset], 2019.
Gattuso, J.-P., Magnan, A. K., Bopp, L., Cheung, W. W., Duarte, C. M., Hinkel, J., Mcleod, E., Micheli, F., Oschlies, A., and Williamson, P.: Ocean solutions to address climate change and its effects on marine ecosystems, Frontiers in Marine Science, 337, 2018.
Gehlen, M., Gangstø, R., Schneider, B., Bopp, L., Aumont, O., and Ethe, C.: The fate of pelagic CaCO3 production in a high CO2 ocean: a model study, Biogeosciences, 4, 505–519, https://doi.org/10.5194/bg-4-505-2007, 2007.
González, M. F. and Ilyina, T.: Impacts of artificial ocean alkalinization on the carbon cycle and climate in Earth system simulations, J Geophys Res, 43, 6493-6502, https://doi.org/10.1002/2016GL068576, 2016.
Guo, H., John, J. G., Blanton, C., McHugh, C., Nikonov, S., Radhakrishnan, A., Rand, K., Zadeh, N. T., Balaji, V., Durachta, J., Dupuis, C., Menzel, R., Robinson, T., Underwood, S., Vahlenkamp, H., Bushuk, M., Dunne, K. A., Dussin, R., Gauthier, P. P. G., Ginoux, P., Griffies, S. M., Hallberg, R., Harrison, M., Hurlin, W., Lin, P., Malyshev, S., Naik, V., Paulot, F., Paynter, D. J., Ploshay, J., Reichl, B. G., Schwarzkopf, D. M., Seman, C. J., Shao, A., Silvers, L., Wyman, B., Yan, X., Zeng, Y., Adcroft, A., Dunne, J. P., Held, I. M., Krasting, J. P., Horowitz, L. W., Milly, P. C. D., Shevliakova, E., Winton, M., Zhao, M., and Zhang, R.: NOAA-GFDL GFDL-CM4 model output historical, Earth System Grid Federation [dataset], 10.22033/ESGF/CMIP6.8594, 2018.
Hartmann, J., Suitner, N., Lim, C., Schneider, J., Marín-Samper, L., Arístegui, J., Renforth, P., Taucher, J., and Riebesell, U.: Stability of alkalinity in Ocean Alkalinity Enhancement (OAE) approaches–consequences for durability of CO 2 storage, Biogeosciences Discussions, 1–29, 2022.
Hauck, J., Köhler, P., Wolf-Gladrow, D., and Völker, C.: Iron fertilisation and century-scale effects of open ocean dissolution of olivine in a simulated CO2 removal experiment, Environmental Research Letters, 11, 024007, 2016.
Held, I. M., Guo, H., Adcroft, A., Dunne, J. P., Horowitz, L. W., Krasting, J., Shevliakova, E., Winton, M., Zhao, M., Bushuk, M., Wittenberg, A. T., Wyman, B., Xiang, B., Zhang, R., Anderson, W., Balaji, V., Donner, L., Dunne, K., Durachta, J., Gauthier, P. P. G., Ginoux, P., Golaz, J.-C., Griffies, S. M., Hallberg, R., Harris, L., Harrison, M., Hurlin, W., John, J., Lin, P., Lin, S.-J., Malyshev, S., Menzel, R., Milly, P. C. D., Ming, Y., Naik, V., Paynter, D., Paulot, F., Rammaswamy, V., Reichl, B., Robinson, T., Rosati, A., Seman, C., Silvers, L. G., Underwood, S., and Zadeh, N.: Structure and Performance of GFDL's CM4.0 Climate Model, Journal of Advances in Modeling Earth Systems, 11, 3691-3727, https://doi.org/10.1029/2019MS001829, 2019.

Ilyina, T., Wolf-Gladrow, D., Munhoven, G., and Heinze, C.: Assessing the potential of calcium-based artificial ocean alkalinization to mitigate rising atmospheric CO2 and ocean acidification, J Geophys Res, 40, 5909-5914, 2013.

Jansen, H. and Wolf-Gladrow, D. A.: Carbonate dissolution in copepod guts: a numerical model, Marine Ecology Progress Series, 221, 199-207, 2001.

Jungclaus, J., Bittner, M., Wieners, K.-H., Wachsmann, F., Schupfner, M., Legutke, S., Giorgetta, M., Reick, C., Gayler, V., Haak, H., de Vrese, P., Raddatz, T., Esch, M., Mauritsen, T., von Storch, J.-S., Behrens, J., Brovkin, V., Claussen, M., Crueger, T., Fast, I., Fiedler, S., Hagemann, S., Hohenegger, C., Jahns, T., Kloster, S., Kinne, S., Lasslop, G., Kornblueh, L., Marotzke, J., Matei, D., Meraner, K., Mikolajewicz, U., Modali, K., Müller, W., Nabel, J., Notz, D., Peters-von Gehlen, K., Pincus, R., Pohlmann, H., Pongratz, J., Rast, S., Schmidt, H., Schnur, R., Schulzweida, U., Six, K., Stevens, B., Voigt, A., and Roeckner, E.: MPI-M MPI-ESM1.2-HR model output prepared for CMIP6 CMIP historical, Earth System Grid Federation [dataset], 10.22033/ESGF/CMIP6.6594, 2019.

Keller, D. P., Feng, E. Y., and Oschlies, A.: Potential climate engineering effectiveness and side effects during a high carbon dioxide-emission scenario, Nature communications, 5, 1-11, 2014.

Keller, D. P., Lenton, A., Scott, V., Vaughan, N. E., Bauer, N., Ji, D., Jones, C. D., Kravitz, B., Muri, H., and Zickfeld, K.: The Carbon Dioxide Removal Model Intercomparison Project (CDRMIP): rationale and experimental protocol for CMIP6, Geosci. Model Dev., 11, 1133-1160, 10.5194/gmd-11-1133-2018, 2018.

Koeve, W., Duteil, O., Oschlies, A., Kähler, P., and Segschneider, J.: Methods to evaluate CaCO3 cycle modules in coupled global biogeochemical ocean models, Geosci. Model Dev., 7, 2393–2408, https://doi.org/10.5194/gmd-7-2393-2014, 2014.

Köhler, P., Abrams, J. F., Völker, C., Hauck, J., and Wolf-Gladrow, D. A.: Geoengineering impact of open ocean dissolution of olivine on atmospheric CO_2 , surface ocean pH and marine biology, Environmental Research Letters, 8, 014009, 10.1088/1748-9326/8/1/014009, 2013.

Krasting, J. P., John, J. G., Blanton, C., McHugh, C., Nikonov, S., Radhakrishnan, A., Rand, K., Zadeh, N. T., Balaji, V., Durachta, J., Dupuis, C., Menzel, R., Robinson, T., Underwood, S., Vahlenkamp, H., Dunne, K. A., Gauthier, P. P. G., Ginoux, P., Griffies, S. M., Hallberg, R., Harrison, M., Hurlin, W., Malyshev, S., Naik, V., Paulot, F., Paynter, D. J., Ploshay, J., Reichl, B. G., Schwarzkopf, D. M., Seman, C. J., Silvers, L., Wyman, B., Zeng, Y., Adcroft, A., Dunne, J. P., Dussin, R., Guo, H., He, J., Held, I. M., Horowitz, L. W., Lin, P., Milly, P. C. D., Shevliakova, E., Stock, C., Winton, M., Wittenberg, A. T., Xie, Y., and Zhao, M.: NOAA-GFDL GFDL-ESM4 model output prepared for CMIP6 CMIP historical, Earth System Grid Federation [dataset], 10.22033/ESGF/CMIP6.8597, 2018.

Kwiatkowski, L., Torres, O., Bopp, L., Aumont, O., Chamberlain, M., Christian, J. R., Dunne, J. P., Gehlen, M., Ilyina, T., and John, J. G.: Twenty-first century ocean warming, acidification, deoxygenation, and upper-ocean nutrient and primary production decline from CMIP6 model projections, Biogeosciences, 17, 3439-3470, 2020.

Lauvset, S. K., Key, R. M., Olsen, A., Van Heuven, S., Velo, A., Lin, X., Schirnick, C., Kozyr, A., Tanhua, T., and Hoppema, M.: A new global interior ocean mapped climatology: The 1× 1 GLODAP version 2, Earth System Science Data, 8, 325-340, 2016.

Lawrence, M. G., Schäfer, S., Muri, H., Scott, V., Oschlies, A., Vaughan, N. E., Boucher, O., Schmidt, H., Haywood, J., and Scheffran, J.: Evaluating climate geoengineering proposals in the context of the Paris Agreement temperature goals, Nature communications, 9, 1-19, 2018.

Lenton, A., Matear, R. J., Keller, D. P., Scott, V., and Vaughan, N. E.: Assessing carbon dioxide removal through global and regional ocean alkalinization under high and low emission pathways, Earth Syst. Dynam., 9, 339-357, 10.5194/esd-9-339-2018, 2018.

Lewis, E., Wallace, D., & Allison, L. J.: Program developed for CO_2 system calculations (No. ORNL/CDIAC-105). Brookhaven National Lab., Dept. of Applied Science, Upton, NY (United States); Oak Ridge National Lab., Carbon Dioxide Information Analysis Center, TN (United States), 1998.

Mauritsen, T., Bader, J., Becker, T., Behrens, J., Bittner, M., Brokopf, R., Brovkin, V., Claussen, M., Crueger, T., and Esch, M.: Developments in the MPI-M Earth System Model version 1.2 (MPI-ESM1. 2) and its response to increasing CO2, Journal of Advances in Modeling Earth Systems, 11, 998-1038, 2019.

Middelburg, J. J., Soetaert, K., and Hagens, M.: Ocean alkalinity, buffering and biogeochemical processes, Reviews of Geophysics, 58, e2019RG000681, 2020.

Millero, F. J., Lee, K., and Roche, M.: Distribution of alkalinity in the surface waters of the major oceans, Marine Chemistry, 60, 111-130, 1998.

Müller, W. A., Jungclaus, J. H., Mauritsen, T., Baehr, J., Bittner, M., Budich, R., Bunzel, F., Esch, M., Ghosh, R., Haak, H., Ilyina, T., Kleine, T., Kornblueh, L., Li, H., Modali, K., Notz, D., Pohlmann, H., Roeckner, E., Stemmler, I., Tian, F., and Marotzke, J.: A Higher-resolution Version of the Max Planck Institute Earth System Model (MPI-ESM1.2-HR), Journal of Advances in Modeling Earth Systems, 10, 1383-1413, https://doi.org/10.1029/2017MS001217, 2018.

National Academies of Sciences, E., and Medicine: A research strategy for ocean-based carbon dioxide removal and sequestration, 2021.

Planchat, A., Kwiatkwoski, L., Bopp, L., Torres, O., Christian, J. R., Butenschön, M., Lovato, T., Séférian, R., Chamberlain, M. A., and Aumont, O.: The representation of alkalinity and the carbonate pump from CMIP5 to CMIP6 ESMs and implications for the ocean carbon cycle, EGUsphere, 1–76, 2022.

Pond, D., Harris, R., and Brownlee, C.: A microinjection technique using a pH-sensitive dye to determine the gut pH of Calanus helgolandicus, Marine Biology, 123, 75-79, 1995.

Renforth, P. and Henderson, G.: Assessing ocean alkalinity for carbon sequestration, Reviews of Geophysics, 55, 636-674, 2017.

Revelle, R. and Suess, H. E.: Carbon dioxide exchange between atmosphere and ocean and the question of an increase of atmospheric CO2 during the past decades, Tellus, 9, 18–27, 1957.

Rogelj, J., Shindell, D., Jiang, K., Fifita, S., Forster, P., Ginzburg, V., Handa, C., Kheshgi, H., Kobayashi, S., and Kriegler, E.: Mitigation pathways compatible with 1.5 C in the context of sustainable development, in: Global warming of 1.5 C, Intergovernmental Panel on Climate Change, 93-174, 2018.

Sabine, C. L., Key, R. M., Feely, R. A., and Greeley, D.: Inorganic carbon in the Indian Ocean: Distribution and dissolution processes, Global Biogeochemical Cycles, 16, 15-11-15-18, 2002.

Salter, M. A., Harborne, A. R., Perry, C. T., & Wilson, R. W.: Phase heterogeneity in carbonate production by marine fish influences their roles in sediment generation and the inorganic carbon cycle. *Scientific Reports*, *7*(1), 765, 2017.

Schulzweida, Uwe.: CDO User Guide (2.1.0). Zenodo. https://doi.org/10.5281/zenodo.7112925, 2022.

Seferian, R.: CNRM-CERFACS CNRM-ESM2-1 model output prepared for CMIP6 CMIP historical, Earth System Grid Federation [dataset], 10.22033/ESGF/CMIP6.4068, 2018.

Séférian, R., Berthet, S., Yool, A., Palmiéri, J., Bopp, L., Tagliabue, A., Kwiatkowski, L., Aumont, O., Christian, J., Dunne, J., Gehlen, M., Ilyina, T., John, J. G., Li, H., Long, M. C., Luo, J. Y., Nakano, H., Romanou, A., Schwinger, J., Stock, C., Santana-Falcón, Y., Takano, Y., Tjiputra, J., Tsujino, H., Watanabe, M., Wu, T., Wu, F., and Yamamoto, A.: Tracking Improvement in Simulated Marine Biogeochemistry Between CMIP5 and CMIP6, Current Climate Change Reports, 6, 95-119, 10.1007/s40641-020-00160-0, 2020.

Séférian, R., Nabat, P., Michou, M., Saint-Martin, D., Voldoire, A., Colin, J., Decharme, B., Delire, C., Berthet, S., Chevallier, M., Sénési, S., Franchisteguy, L., Vial, J., Mallet, M., Joetzjer, E., Geoffroy, O., Guérémy, J.-F., Moine, M.-P., Msadek, R., Ribes, A., Rocher, M., Roehrig, R., Salas-y-Mélia, D., Sanchez, E., Terray, L., Valcke, S., Waldman, R., Aumont, O., Bopp, L., Deshayes, J., Éthé, C., and Madec, G.: Evaluation of CNRM Earth System Model, CNRM-ESM2-1: Role of Earth System Processes in Present-Day and Future Climate, Journal of Advances in Modeling Earth Systems, 11, 4182-4227, https://doi.org/10.1029/2019MS001791, 2019.

Seland, Ø., Bentsen, M., Oliviè, D. J. L., Toniazzo, T., Gjermundsen, A., Graff, L. S., Debernard, J. B., Gupta, A. K., He, Y., Kirkevåg, A., Schwinger, J., Tjiputra, J., Aas, K. S., Bethke, I., Fan, Y., Griesfeller, J., Grini, A., Guo, C., Ilicak, M., Karset, I. H. H., Landgren, O. A., Liakka, J., Moseid, K. O., Nummelin, A., Spensberger, C., Tang, H., Zhang, Z., Heinze, C., Iversen, T., and Schulz, M.: NCC NorESM2-LM model output prepared for CMIP6 CMIP historical, Earth System Grid Federation [dataset], 10.22033/ESGF/CMIP6.8036, 2019.

Sellar, A. A., Jones, C. G., Mulcahy, J. P., Tang, Y., Yool, A., Wiltshire, A., O'connor, F. M., Stringer, M., Hill, R., and Palmieri, J.: UKESM1: Description and evaluation of the UK Earth System Model, Journal of Advances in Modeling Earth Systems, 11, 4513-4558, 2019.

Smith, P., Davis, S. J., Creutzig, F., Fuss, S., Minx, J., Gabrielle, B., Kato, E., Jackson, R. B., Cowie, A., and Kriegler, E.: Biophysical and economic limits to negative CO2 emissions, Nature climate change, 6, 42-50, 2016.

Sulpis, O., Jeansson, E., Dinauer, A., Lauvset, S. K., and Middelburg, J. J.: Calcium carbonate dissolution patterns in the ocean, Nature Geoscience, 14, 423–428, https://doi.org/10.1038/s41561-021-00743-y, 2021.

Steele, M., Morley, R., and Ermold, W.: PHC: A global ocean hydrography with a high-quality Arctic Ocean, Journal of Climate, 14, 2079-2087, 2001.

Swart, N. C., Cole, J. N. S., Kharin, V. V., Lazare, M., Scinocca, J. F., Gillett, N. P., Anstey, J., Arora, V., Christian, J. R., Jiao, Y., Lee, W. G., Majaess, F., Saenko, O. A., Seiler, C., Seinen, C., Shao, A., Solheim, L., von Salzen, K., Yang, D., Winter, B., and Sigmond, M.: CCCma CanESM5 model output prepared for CMIP6 CMIP historical, Earth System Grid Federation [dataset], 10.22033/ESGF/CMIP6.3610, 2019a.

Swart, N. C., Cole, J. N. S., Kharin, V. V., Lazare, M., Scinocca, J. F., Gillett, N. P., Anstey, J., Arora, V., Christian, J. R., Hanna, S., Jiao, Y., Lee, W. G., Majaess, F., Saenko, O. A., Seiler, C., Seinen, C., Shao, A., Sigmond, M., Solheim, L., von Salzen, K., Yang, D., and Winter, B.: The Canadian Earth System Model version 5 (CanESM5.0.3), Geosci. Model Dev., 12, 4823-4873, 10.5194/gmd-12-4823-2019, 2019b.

Tagliabue, A., Kwiatkowski, L., Bopp, L., Butenschön, M., Cheung, W., Lengaigne, M., and Vialard, J.: Persistent Uncertainties in Ocean Net Primary Production Climate Change Projections at Regional Scales Raise Challenges for Assessing Impacts on Ecosystem Services, Frontiers in Climate, 3, 10.3389/fclim.2021.738224, 2021.

Takahashi, T., Broecker, W. S., and Bainbridge, A. E.: The alkalinity and total carbon dioxide concentration in the world oceans, Carbon cycle modelling, SCOPE, 16, 271–286, 1981.

Talley, L. D.: Salinity patterns in the ocean, The Earth system: physical and chemical dimensions of global environmental change, 1, 629–640, 2002.

Tang, Y., Rumbold, S., Ellis, R., Kelley, D., Mulcahy, J., Sellar, A., Walton, J., and Jones, C.: MOHC UKESM1.0-LL model output prepared for CMIP6 CMIP historical, Earth System Grid Federation [dataset], 10.22033/ESGF/CMIP6.6113, 2019.

Terhaar, J., Frölicher, T. L., and Joos, F.: Observation-constrained estimates of the global ocean carbon sink from Earth system models, Biogeosciences, 19, 4431–4457, https://doi.org/10.5194/bg-19-4431-2022, 2022.

Tjiputra, J. F., Schwinger, J., Bentsen, M., Morée, A. L., Gao, S., Bethke, I., Heinze, C., Goris, N., Gupta, A., He, Y. C., Olivié, D., Seland, Ø., and Schulz, M.: Ocean biogeochemistry in the Norwegian Earth System Model version 2 (NorESM2), Geosci. Model Dev., 13, 2393-2431, 10.5194/gmd-13-2393-2020, 2020.

Van Heuven, S., Pierrot, D., Rae, J., Lewis, E., and Wallace, D.: MATLAB program developed for CO2 system calculations, ORNL/CDIAC-105b, 530, 2011.

Weiss, R.F.: The solubility of nitrogen, oxygen and argon in water and seawater, Deep sea research and oceanographic abstracts, 721-735, 1970.

White, M. M., Waller, J. D., Lubelczyk, L. C., Drapeau, D. T., Bowler, B. C., Balch, W. M., and Fields, D. M.: Coccolith dissolution within copepod guts affects fecal pellet density and sinking rate, Scientific RepoRtS, 8, 1-6, 2018.

Wieners, K.-H., Giorgetta, M., Jungclaus, J., Reick, C., Esch, M., Bittner, M., Legutke, S., Schupfner, M., Wachsmann, F., Gayler, V., Haak, H., de Vrese, P., Raddatz, T., Mauritsen, T., von Storch, J.-S., Behrens, J., Brovkin, V., Claussen, M., Crueger, T., Fast, I., Fiedler, S., Hagemann, S., Hohenegger, C., Jahns, T., Kloster, S., Kinne, S., Lasslop, G., Kornblueh, L., Marotzke, J., Matei, D., Meraner, K., Mikolajewicz, U., Modali, K., Müller, W., Nabel, J., Notz, D., Peters-von Gehlen, K., Pincus, R., Pohlmann, H., Pongratz, J., Rast, S., Schmidt, H., Schnur, R., Schulzweida, U., Six, K., Stevens, B., Voigt, A., and Roeckner, E.: MPI-M MPI-ESM1.2-LR model output prepared for CMIP6 CMIP historical, Earth System Grid Federation [dataset], 10.22033/ESGF/CMIP6.6595, 2019.

Yamanaka, Y. and Tajika, E.: The role of the vertical fluxes of particulate organic matter and calcite in the oceanic carbon cycle: Studies using an ocean biogeochemical general circulation model, Global Biogeochemical Cycles, 10, 361–382, 1996.

Yukimoto, S., Kawai, H., Koshiro, T., Oshima, N., Yoshida, K., Urakawa, S., Tsujino, H., Deushi, M., Tanaka, T., and Hosaka, M.: The Meteorological Research Institute Earth System Model version 2.0, MRI-ESM2. 0: Description and basic evaluation of the physical component, Journal of the Meteorological Society of Japan. Ser. II, 2019a.

Yukimoto, S., Koshiro, T., Kawai, H., Oshima, N., Yoshida, K., Urakawa, S., Tsujino, H., Deushi, M., Tanaka, T., Hosaka, M., Yoshimura, H., Shindo, E., Mizuta, R., Ishii, M., Obata, A., and Adachi, Y.: MRI MRI-ESM2.0 model output prepared for CMIP6 CMIP historical, Earth System Grid Federation [dataset], 10.22033/ESGF/CMIP6.6842, 2019b.

Zeebe, R. E. and Wolf-Gladrow, D.: CO2 in seawater: equilibrium, kinetics, isotopes, Gulf Professional Publishing, 2001.

Ziehn, T., Chamberlain, M. A., Law, R. M., Lenton, A., Bodman, R. W., Dix, M., Stevens, L., Wang, Y.-P., and Srbinovsky, J.: The Australian earth system model: ACCESS-ESM1. 5, Journal of Southern Hemisphere Earth Systems Science, 70, 193-214, 2020.

Ziehn, T., Chamberlain, M., Lenton, A., Law, R., Bodman, R., Dix, M., Wang, Y., Dobrohotoff, P., Srbinovsky, J., Stevens, L., Vohralik, P., Mackallah, C., Sullivan, A., O'Farrell, S., and Druken, K.: CSIRO ACCESS-ESM1.5 model output prepared for CMIP6 CMIP historical, Earth System Grid Federation [dataset], 10.22033/ESGF/CMIP6.4272, 2019.